Electrical Power and Energy Systems 155 (2024) 109519

Contents lists available at ScienceDirect

International Journal of Electrical Power and Energy Systems

journal homepage: www.elsevier.com/locate/ijepes

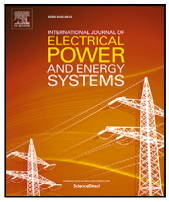

Power system resilience against climatic faults: An optimized self-healing approach using conservative voltage reduction

Rawdha H. AlKuwaiti [a,*,1], Wael T. El-Sayed [b,1], Hany E.Z. Farag [c,1], Ahmed Al-Durra [a,1], Ehab F. El-Saadany [a,1]

[a] Advanced Power and Energy Center, APEC, Khalifa University, Abu Dhabi, United Arab Emirates
[b] Electrical Engineering Department, Faculty of Engineering at Shoubra, Benha University, Cairo, Egypt
[c] Electrical Engineering and Computer Science Department, York University, Ontario, Canada M3J1P3

ARTICLE INFO

Keywords:
Conservative voltage reduction
Optimization
Power system resilience
Reconfiguration
Self-healing

ABSTRACT

The resilience of power systems is critical in mitigating faults caused by the impending effects of climate change. Typical operational methods, such as network reconfiguration, may be insufficient to mitigate faults in the event of a contingency. On the other hand, reducing system demand may help increase the number of restored loads. As a result, this paper proposes a novel self-healing optimization approach based on a power grid concept known as conservative voltage reduction (CVR), which results in system demand reduction. The proposed optimization model is formulated as a mixed integer non-linear (MINLP) problem to fulfill an objective of minimizing unserved loads within the system. Voltage, thermal capacity, system radiality, and several more constraints have been taken into consideration while formulating the proposed model to handle both grid-connected and isolated modes of operation. Both dispatchable and non-dispatchable distributed generators (DGs) are taken into consideration. Dispatchable DGs are assumed to be capable of switching back and forth between constant power (PQ) and droop controls for the purpose of grid following and grid forming in grid-connected and isolated modes of operation, respectively. The proposed optimization approach is coded and solved using the General Algebraic Modeling System (GAMS) software. The IEEE 69-bus power distribution test system is utilized to test the validity and superiority of the proposed model. The results show that the proposed model effectively increases the system resilience by reducing the unserved power/energy within the system following a contingency.

1. Introduction

The frequent occurrence of unusual severe weather conditions caused by the climate change have had significant impacts on the operation of power systems, resulting in repetitive system faults, blackouts, and other devastating impacts on communities [1]. As such, improving the power system resiliency during such extreme weather events have become utilities' top priority causing them to place strategies/schemes accordingly [2,3]. Enhancement of the system resilience is typically addressed through operational and hardening restoration procedures. Hardening procedures involve improving the system's physical aspects while operational measures deal with controlling the system in a way to make it less susceptible to faults [4]. The deployment of innovative self-healing solutions are expected to offer power utilities the tools needed to significantly enhance the grid resiliency under these extreme events. Fault detection, isolation, and service restoration (FDIR) are the essential elements of any self-healing solution [5]. In this regard, once self-healing is deployed, power utilities would be able to automatically locate and isolate permanent faults in the grid. However, in many cases, some loads are left behind and disconnected due to the fault clearance. Furthermore, a load shedding mechanism is typically activated when there is no adequate supply from the main grid and/or the local distributed generation (DG) [6]. The final step of a successful self-healing mechanism attempts to restore the service to the impacted loads, typically by reconfiguration, which is achieved by finding the optimal topology that maximizes the restored loads while respecting the imposed system limits [7].

Network reconfiguration is a process commonly associated with load restoration following a fault, where it has significantly contributed to the improvement of power system resilience by rerouting faulty regions to other supply sources using sectionalizing switches within a

* Corresponding author.
E-mail address: 100058229@ku.ac.ae (R.H. AlKuwaiti).
[1] All authors have contributed equally to this research.

https://doi.org/10.1016/j.ijepes.2023.109519
Received 3 March 2023; Received in revised form 18 August 2023; Accepted 17 September 2023
Available online 28 September 2023

Nomenclature

Indices

i	Sending node index.
j	Receiving node index.
s	Probabilistic states index.
u	Distributed generator index.
w	Wind turbine index.

Variables

$Q^{s}_{load,i}$	Reactive power consumed at each node i for each state s.
$\omega^{s,lb}$	Lower bound of the system frequency at each state s.
$\omega^{s,nom}_{DG,i}$	Nominal angular frequency of the DG connected to node i at each state s.
$\omega^{s,ub}$	Upper bound of the system frequency at each state s.
ω^{s}	Global system frequency at each state s.
$m^{s}_{p,DG}$	Active droop gain of node connected to a DG for each state s.
$n^{s}_{q,DG}$	Reactive droop gain of node connected to a DG for each state s.
$P^{s,u}_{DG,i}$	Active power generated by dispatchable distributed generation u at each node i for each state s.
$P^{s}_{grid,i}$	Active power generated by grid at each node i for each state s.
$P^{s}_{load,i}$	Active power consumed at each node i for each state s.
$P^{s}_{US,i}$	Unserved active power for every node i in each state s.
$Q^{s,u}_{DG,i}$	Reactive power generated by dispatchable distributed generation u at each node i for each state s.
$Q^{s}_{grid,i}$	Reactive power generated by grid at each node i for each state s.
$Q^{s}_{US,i}$	Unserved reactive power for every node i in each state s.
v^{s}_{o}	Base voltage at each state s.
$v^{s,nom}_{DG,i}$	Nominal voltage of the DG connected to node i at each state s.
v_{OLTC}	On load tap changer voltage setpoint.
x^{s}_{i}	Control variable determining the portion of unserved power for every node i, in each state s.

feeder or tie switches between feeders [8,9]. Numerous techniques are proposed in the literature to find the optimal reconfiguration of a power distribution system for the purpose of load restoration while satisfying a variety of objectives. The work in [7] proposes service restoration methods with partial objectives of reducing losses. Minimizing the cost of losses is one of the five-part objective presented in [7]. The authors of [10] suggest a multi-objective multi-constraint strategy for service restoration. While restoring the service, the authors of [10,11] considered customer priorities as well as manual and remotely operated switches. The multi-objective strategy in [10] considers minimizing losses as one of its objectives although including loss minimization within the objective could conflict with the load restoration operation [11]. In efforts to reconnect as many loads as possible after a fault, fuzzy multiagent systems approach was utilized in [12]. This approach was based on a hybrid centralized-decentralized control system developed to increase the system's flexibility and resilience. However, the technique in [12] relies heavily on communication infrastructure, which must be optimized. The work in [13] uses a rolling-horizon optimization strategy to schedule DGs in normal and self-healing operations. Normal operations seek to maximize revenue while minimizing costs. In contrast, self-healing operations divide the system into networked self-supplied microgrids to provide service continuity to as many loads as possible. The authors in [13] also considered non-dispatchable DGs as a two-stage stochastic optimization problem. Disturbance-dependent islanding schemes are used in [13–16] to divide the system into smaller islands in response to a fault in the system, where the islands proposed in [14] are not necessarily self-sufficient as they are formed based on an automated response to a fault and, thus, significant load shedding is expected. In [15], a two-stage dynamic microgrid operation scheme is proposed. The proposed scheme starts off by disconnecting the system from the main grid then splitting it into several microgrids following a blackout. In order to initiate the black start, the created microgrids are then reconfigured and sequentially reconnected together to eventually represent the distribution system again and connect it back to the main grid. However, the work in [15] does not examine the system's sequence of black-start restoration procedure while [16] has proposed a black-start restoration model that considers the sequence of restoration. The black-start model has been formulated as a mixed-integer second-order cone program. Here it is noteworthy that blackouts are not expected to occur on a regular basis because of climate change [17,18] as they are a result of highly severe weather conditions or faults. On the other hand, brownouts occur more commonly as they require a much smaller disturbance to initiate. A distribution system's radial configuration provides the system with a simple design, however, a failure of any of the system's parts could result in an outage for all downstream loads [5]. Distribution systems are typically equipped with tie-lines, thus having the option to reconfigure to achieve different objectives such as loss reduction, improve voltage profile and most importantly restore shed loads under contingency situations. Nonetheless, the system imposes restrictions such as voltage and line rating limitations that could hinder reconfiguration's ability to restore lost loads. The ability of a resilient system to recover lost load is one of its most essential characteristics [8]. In this regard, reducing the served customers' power demand may help increase the number of restored loads. Without the need of direct communication and control of the customers' load, power utilities should be able to reduce the power demanded by the served customers using the concept of conservative voltage reduction (CVR). CVR techniques aim to minimize the voltage on the system buses without violating the lower limit, which in turn reflects in reducing the power consumed on those buses, given that they are voltage dependent loads. Upon implementing CVR to the system, more power is freed up as the served loads start consuming less power. Potentially, implying a proportional increase in reconfiguration's range of operation and restoring more loads proportional to the power freed up by implementing CVR. Consequently, this paper proposes to combine the concept of CVR alongside the load restoration process to produce a novel and more efficient self-healing scheme. The previously mentioned literature has not explored voltage control for the purpose of load restoration, which is a method of implementing CVR, within their networked microgrids. CVR is a popular method for lowering the power demand in distribution networks by reducing the voltage across the network [19]. It is typically used in situations such as unintentional islanding, a sudden increase in demand, or a sudden decrease in system generation. These events typically result in load shedding, but with CVR, load shedding can be reduced. The method is also versatile enough to be used for demand side management and in coordinating microgrid DG's voltage and reactive power (volt/var) control. The authors in [20] have established a mixed-integer nonlinear programming (MINLP) problem to reduce the power demand across

the network using volt/var control. The objectives of the proposed volt/var control in [20] is energy saving and minimizing losses within the system, however, the impacts of such control on the load restoration process is not taken into consideration.

It is generally noted from the literature survey that considerable efforts have been done with respect to optimizing the load restoration process using different techniques; however, none of the work presented has considered the benefits that volt/var control mechanisms, such as CVR, could bring when applied in conjunction with the restoration process. The efforts done in enhancing the self-healing scheme included solely reconfiguration and islanding-based techniques [7,10–14].

Based on the above discussion, this paper aims to integrate the concept of CVR within the service restoration optimization process for power distribution systems to maximize the number of restored loads. Both dispatchable and non-dispatchable DGs are incorporated into the model. Dispatchable DGs are assumed to be capable of switching back and forth between constant active and reactive (PQ) and droop controls for the purpose of grid following and grid forming in grid-connected and isolated modes of operation, respectively. The proposed integrated optimization model is formulated as a mixed integer nonlinear (MINLP) problem with consideration of both grid-connected and isolated modes of operation. This paper's main contributions are the following:

1. Formulating a new optimization model to enhance the system resilience against climactic faults by integrating the CVR concept in the service restoration process.
2. Proving the framework's universal implementation by consideration of different system modes: Grid-connected & Isolated system, with the addition of dispatchable and non-dispatchable DGs.
3. Exploring a probabilistic approach in modeling the uncertainty of the system load and variable DGs, and creating annual assessment of the proposed approach over all of the probabilistic system states.

The rest of the paper is organized as follows: Section 2 presents the model formulation of the proposed optimization approach. The approach is tested and analyzed using four case studies in Section 3 and lastly Section 4 concludes the work and summarizes its main contributions.

2. Proposed optimization model

This section presents the MINLP formulation of the proposed approach. The formulation's objective is to minimize the total unserved power/shed load, $P^s_{US,i}$, in the system as expressed in Eq. (1). The formulated model is generalized to fit both deterministic and probabilistic analysis. The deterministic analysis assumes one state, $m = 1$, in which all the different aspects of the system are operating at rated power while during probabilistic analysis several states are introduced. For every node i at each state s, Eq. (2) defines the unserved power to be a product of the rated load power, $P^s_{load,i}$, multiplied by the control variable, x^s_i, and the load model function, $f^{s,p}(v_i)$. The control variable, x^s_i, is defined in Eq. (3) to be within 0 and 1, where 0 indicates that the load at point i is fully restored and 1 means it is fully unserved.

Exponential and polynomial load models are used interchangeably to model the system load defining the active and reactive load model function in Eqs. (4) & (5). This allows the load to change according to the exponents, α&β, chosen for exponential load modeling while the polynomial load model depends on it is coefficients: Z_p, Z_q, I_p, I_q, P_p & P_q. Lastly, The loads are assumed to be restored in proportion to the load's power factor as reflected in Eq. (6), representing reactive power unserved, $Q^s_{US,i}$ for every node i at each state s. Therefore, the restored active and reactive power of a load will always maintain the load's power factor.

$$\text{Min} \sum_{s=1}^{m}\sum_{i=1}^{n} P^s_{US,i} \tag{1}$$

where,

$$P^s_{US,i} = x^s_i \times P^s_{load,i}(f^{s,p}(v_i)) \tag{2}$$

$$0 \le x^s_i \le 1 \tag{3}$$

$$f^{s,p}(v^s_i) = \begin{cases} (\frac{v^s_i}{v^s_o})^{\alpha} \\ (Z_p(\frac{v^s_i}{v^s_o})^2 + I_p(\frac{v^s_i}{v^s_o}) + P_p) \end{cases} \tag{4}$$

$$f^{s,q}(v^s_i) = \begin{cases} (\frac{v^s_i}{v^s_o})^{\beta} \\ (Z_q(\frac{v^s_i}{v^s_o})^2 + I_q(\frac{v^s_i}{v^s_o}) + P_q) \end{cases} \tag{5}$$

$$Q^s_{US,i} = P^s_{US,i}(\frac{Q^s_{load,i}(f^{s,q}(v_i))}{P^s_{load,i}(f^{s,p}(v_i))}) \tag{6}$$

where n is the total number of buses in the system.

The objective stated in Eq. (1) is subject to the constraints described in the next subsections.

2.1. Power balance constraints

For every node i at each state s, the active and reactive power balance equations, (on the right-hand side) of Eqs. (7)–(8), are defined as nonlinear equality constraints, where the injected power to the node must equal the difference between the generation and load (on the left-hand side) of Eqs. (7)–(8). D is a binary variable that is defined according to the system mode of operation, i.e. grid-connected or isolated. The variable D is assigned as 1 during grid-connected mode and 0 for isolated mode. For every node i at each state s, the generation and load mismatch at that node defines the value of the unserved power of the node as shown in Eqs. (7)–(8) and can be summarized in the variables PF^s_{ij} & QF^s_{ij}.

$$D \times P^s_{grid,i} + \sum_{u=1}^{k} P^{s,u}_{DG,i} - P^s_{load,i} + P^s_{US,i} = \sum_{j=1}^{n} v^s_i \times v^s_j \times Y^s_{i,j} \times \cos(\theta^s_{i,j} + \delta^s_j - \delta^s_i) = PF^s_{ij} \quad \forall i,j,s \tag{7}$$

$$D \times Q^s_{grid,i} + \sum_{u=1}^{k} Q^{s,u}_{DG,i} - Q^s_{load,i} + Q^s_{US,i} = \sum_{j=1}^{n} v^s_i \times v^s_j \times Y^s_{i,j} \times \sin(\theta^s_{i,j} + \delta^s_j - \delta^s_i) = QF^s_{ij} \quad \forall i,j,s \tag{8}$$

where for each state s, $Y^s_{i,j}$ and $\theta^s_{i,j}$ represent the magnitude and angle of the admittance matrix at element ij. δ^s_i and δ^s_j are the power angles associated with node i and j. Lastly, v^s_i and v^s_j are the voltage at node i and j for each state s.

2.2. Main grid & OLTC constraints

The main grid is connected to bus 1 of the system through an on-load tap changer (OLTC). The grid's power ranges are defined using Eqs. (9)–(10) whereas the OLTC is comprised of 16 steps ranging from 0.95 pu to 1.05 pu (in increments of 0.625%) as shown in Eq. (11). The OLTC facilitates CVR application, in a grid-connected system, by determining the optimal number of taps that meets the objectives and constraints of the model. The voltage on bus 1 is set to 1 pu (0 taps) unless CVR is applied.

$$P^{s,min}_{grid} \le P^s_{grid} \le P^{s,max}_{grid} \tag{9}$$

$$Q^{s,min}_{grid} \le Q^s_{grid} \le Q^{s,max}_{grid} \tag{10}$$

$$v_{OLTC} = 1 - taps \times 0.00625 \tag{11}$$

where *taps* represents the optimal tap setting from the 16 taps available to the OLTC (−8 to +8).

2.3. Power generation constraints: Distributed Generation (DGs)

The DG's injected active and reactive power limits are defined using Eqs. (12)–(13), respectively. The dispatchable DGs present in the system are controlled using PQ control in grid-connected mode. It is assumed that the DGs are not allowed to control the voltage during grid-connected mode (grid-following). Alternatively, droop control is used to control the DGs in grid-forming mode (isolated mode) permitting the DGs to control the system's frequency and voltage setpoints as described below in Section 2.7. As for the non-dispatchable DGs, they follow the percentage peak power that is defined in every state and are directly injected into the system.

$$P^{s,u}_{DG,min} \le P^{s,u}_{DG} \le P^{s,u}_{DG,max} \tag{12}$$

$$Q^{s,u}_{DG,min} \le Q^{s,u}_{DG} \le Q^{s,u}_{DG,max} \tag{13}$$

2.4. Thermal constraints

The thermal constraint as shown in Eq. (14) within a system ensure that a line capacity is respected, this is an important constraint for the reconfiguration operation as it limits the restoration path options available and forces the reconfiguration topology to be optimum.

$$(PF^s_{ij})^2 + (QF^s_{ij})^2 \le LS^s_{ij} \times (SF^{s,max}_{ij})^2 \tag{14}$$

where, PF^s_{ij}, QF^s_{ij}, $SF^{s,max}_{ij}$ and LS^s_{ij} are the active, reactive, maximum apparent power flow, and line status for each line ij for each state s.

2.5. Radiality constraints

Ensuring radiality within radial distribution systems is essential to their function. Eq. (15) shows that for each possible loop $\mathcal{L}$ within the distribution system, LS^s_{ij}, line status for each line ij, is the number of buses in the line excluding the open line, therefore ensuring the system's radiality and eliminating any loops. $N_{\mathcal{L}}$ representing the number of lines within a possible loop radial systems. Usually the normally open line is the tie-line that radial distribution systems are equipped with but during reconfiguration the open line within each possible loop will change to reflect the optimal topology.

$$\sum_{i,j \in \mathcal{L}} LS^s_{ij} = N_{\mathcal{L}} - 1 \tag{15}$$

2.6. Voltage constraints

The permissible voltage range is shown in Eq. (16), the range in per unit is chosen according to IEEE standards [21].

$$v^s_{i,min} \le v^s_i \le v^s_{i,max} \tag{16}$$

where the minimum voltage, $v^s_{i,min}$, and maximum voltage, $v^s_{i,max}$, are defined as 0.95 pu & 1.05 pu.

2.7. Isolated system - Additional constraints

2.7.1. Droop control constraints

In grid–connected mode, dispatchable DGs operate in the grid following (PQ) mode given that the main grid holds the system frequency and voltage magnitude. In isolated (grid–forming) mode, dispatchable DG units are responsible of holding the system frequency and bus voltages. Usually, a droop control approach is applied to share the active and reactive power among the dispatchable DG units while holding the system frequency and local bus voltages [22]. Eq. (17) manages active power-sharing based on the frequency of the microgrid while Eq. (18) governs the reactive power-sharing based on the voltage level at the DG's bus.

$$\omega^s = \omega^{s,nom}_{DG,i} - m_{p,DG} \times P^{s,u}_{DG,i} \tag{17}$$

$$v^s_i = v^{s,nom}_{DG,i} - n_{q,DG} \times Q^{s,u}_{DG,i} \qquad \forall i \in DG \tag{18}$$

The nominal voltage setpoint, $v^{s,nom}_{DG,i}$, in Eq. (18) is left to be determined by the optimizer within the voltage range described in Eq. (16) during CVR application, otherwise it is fixed at the upper bound of the voltage range, 1.05 pu.

According to the DG's capacity, the active and reactive power droop gains are adjusted to ensure equal power-sharing. Where $P^{s,u}_{DG,i}$ and $Q^{s,u}_{DG,i}$ are the active and reactive power measurements at node i for every state s, respectively. The active and reactive droop gains, $m^s_{p,DG}$ and $n^s_{q,DG}$, are derived from the upper and lower bounds of frequency and voltage as shown in Eqs. (16), (19)–(21) [23].

$$\omega^{s,lb} \le \omega^s \le \omega^{s,ub} \tag{19}$$

$$m_{p,DG} = \left(\frac{\omega^{s,ub} - \omega^{s,lb}}{P^{s,u}_{DG,max}}\right) \tag{20}$$

$$n_{q,DG} = \left(\frac{v^s_{i,min} - v^s_{i,max}}{Q^{s,u}_{DG,max}}\right) \tag{21}$$

3. Case studies

This section aims to validate the effectiveness of integrating the CVR concept in the optimization of service restoration. To that end, the proposed optimization model has been coded and solved on General Algebraic Modeling System (GAMS), a commonly used optimization software that deals with solving a wide variety of optimization problems [24]. Several system configurations are investigated using the proposed approach, including grid-connected and isolated systems. As discussed earlier, the implementation of CVR varies based on the system configuration; the OLTC has been used at the main grid substation to implement CVR in the presence of the grid. On the other hand, optimizing the nominal voltage of the Q–V droop equations on dispatchable DGs achieves CVR application in isolated system configurations. Load to voltage (LTV) is commonly associated with CVR; essentially it represents the load's voltage dependency/sensitivity. As such, different load types have been investigated for each case study demonstrating how CVR's effect varies from one type to the next. Without loss of generality, the load types investigated in these case studies are: constant power (P), constant current (I), constant impedance (Z) and polynomial load (ZIP) representing a mix of loads in the system.

The 69–bus test system given in [25] has been utilized to demonstrate the effectiveness of the proposed approach. The nominal voltage of the system's feeder is 12.66 kV and the total system active and reactive power load are 3.8 MW and 2.69 MVAR, respectively. The system is comprised of 68 lines and 5 tie lines. Three different cases have been presented in this section, where each case considers the IEEE – 69 bus system with a fault on a bus, but in different conditions as shown in Figs. 1, 2, 4 & 7. Each case is formulated to reflect the effects of climate change and faults it can cause within the system. In some cases, the fault defined is a bus fault in all cases, the faulted bus could have a DG connected to it resulting in generation loss as well. Here it is noteworthy that the simulated faults are selected to cause a portion of the load to be disconnected without creating a complete blackout for the entire system. As such, the concept of cold load pickup, which is usually associated with distribution systems as they recover from blackouts/prolonged outages [26], is not taken into account during the proposed restoration process.

Different operations of the system have been considered to assess the fault: grid-connected system without and with DGs, isolated system with dispatchable DGs and lastly, isolated system with a mix of dispatchable DGs and non-dispatchable DGs.

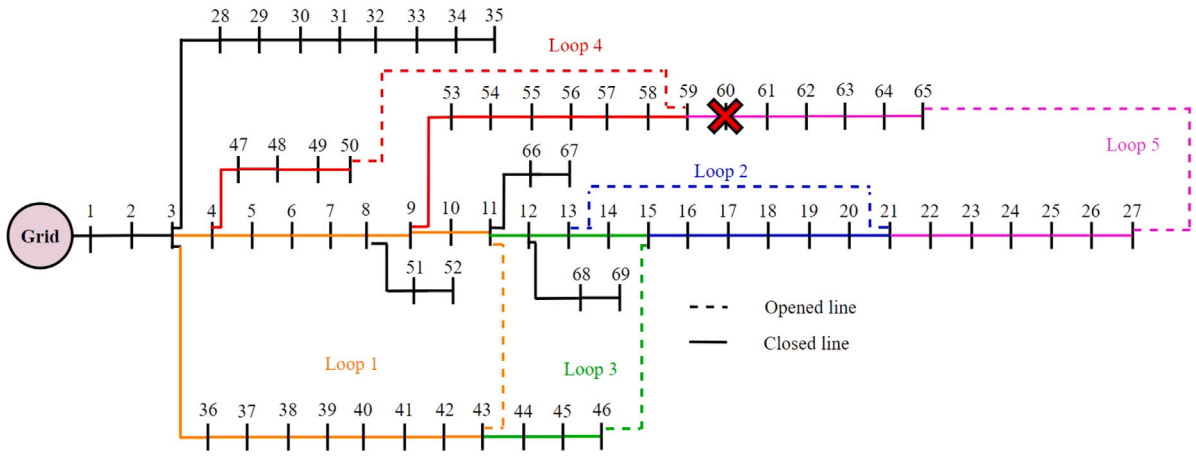

Fig. 1. Grid-connected conventional IEEE 69 bus system without DGs: Fault at bus 60.

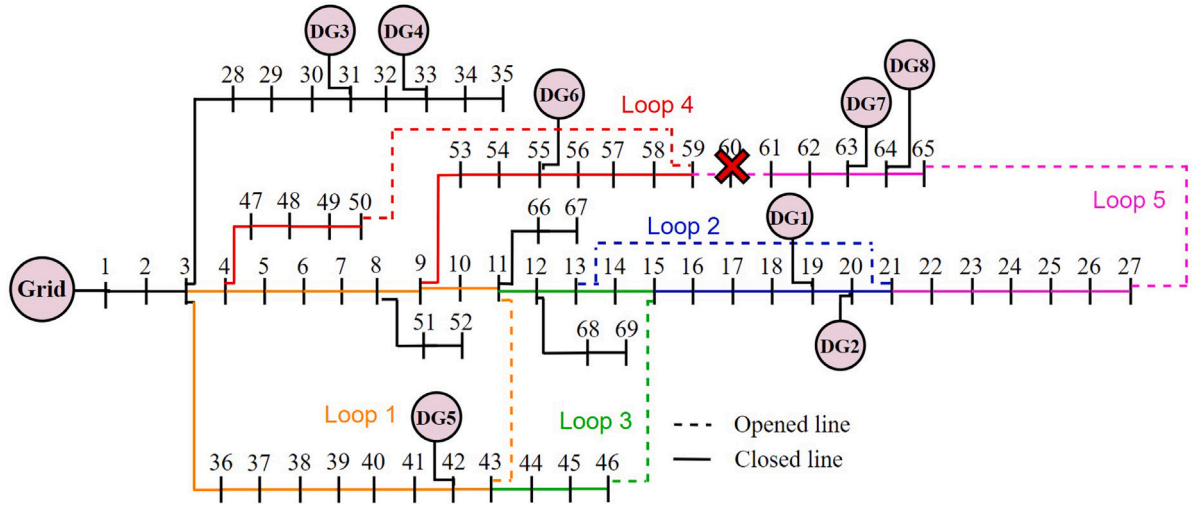

Fig. 2. Grid-connected conventional IEEE 69 bus system with DGs: Fault at bus 60.

The diversity taken into consideration with the system conditions and fault severity reflects different behavior of faults caused by climate change as they range from causing minor to more significant impacts on the system. Similar to how the climatic faults simulated in [8] disconnected roughly a third of the system load, climatic faults in a grid-connected system are defined within these case studies as a bus fault that result in disconnection of a substantial portion (third) of the load. However, unlike grid-connected systems, isolated systems are not expected be severely impacted by the same fault due to the distributed generation present. Therefore, the fault simulated for an isolated system is a fault on a bus connected to a DG, resulting in losing a portion of generation. The following case studies results are formatted uniformly as they examine the power demand lost due to the fault (unserved power demand), the power recovered because of the reconfiguration alone, and the power recovered by utilizing the reconfiguration-CVR fusion. The cases mentioned have been carried out with the following assumptions:

- All loads are reconnected with the same power factor they had initially before the restoration process shown in Eqs. (2)–(6).
- The thermal limits of the system are respected as shown in Eq. (14) [27].
- Permissible ±5% voltage change within the system, reflected within Eq. (16).
- All loads in the system have the same priority.

Table 1
ZIP coefficients for industrial and residential loads [20,28].

	Polynomial coefficients					
	Z_p	Z_q	I_p	I_q	P_p	P_q
Industrial	1.21	4.35	−1.61	−7.08	1.41	3.72
Residential	1.42	8.86	−2.17	−14.59	1.75	6.73

- Constant power load is modeled using exponential load model with $\alpha = \beta = 0$. Constant current load using $\alpha = \beta = 1$ and constant impedance load using $\alpha = \beta = 2$.
- For the system dominated with polynomial (ZIP) load, the loads that have a demand higher than 100 kW are considered industrial while the rest of the loads are considered residential load type. The loads are modeled according to the coefficients defined in Table 1.
- System bases:
  - Base Apparent Power: 10 MVA
  - Base Voltage: 12.66 kV

3.1. Case 1: Grid–connected system

In this case study, it is assumed that the studied 69–bus distribution system operates in grid-connected mode. A single fault occurring at bus

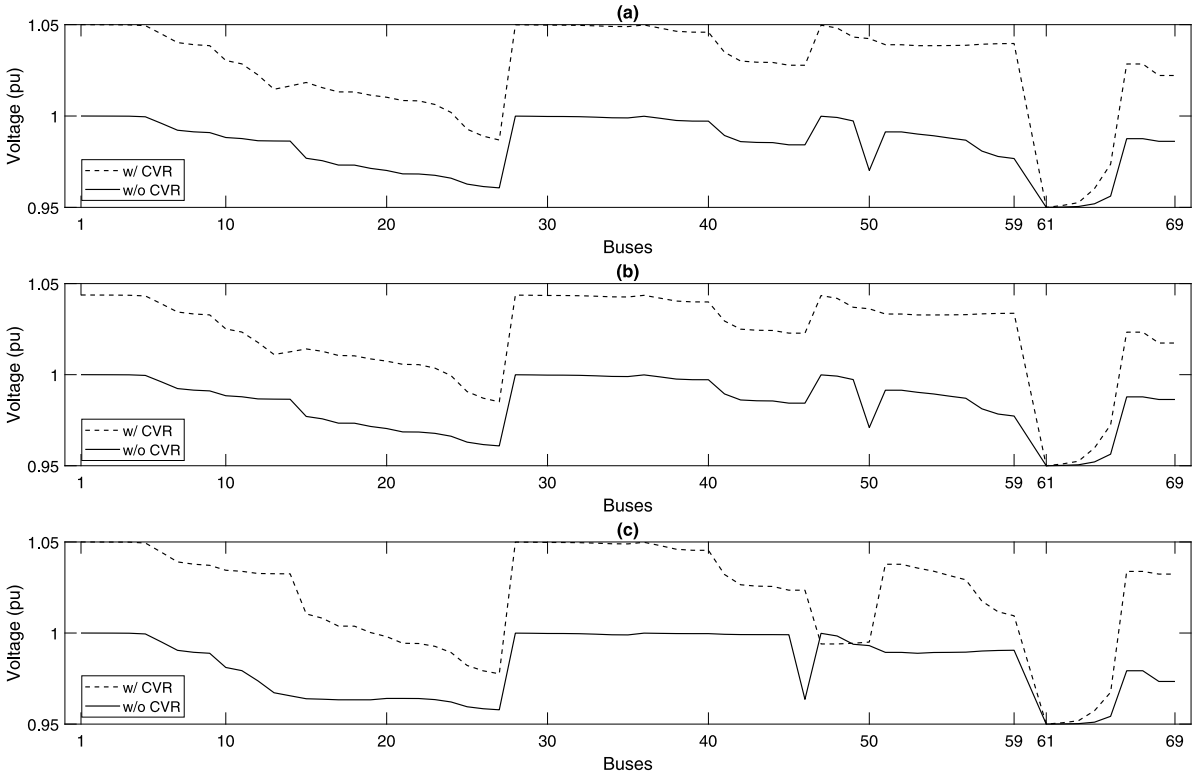

Fig. 3. Case 1 (a) voltage profile for: (a) constant current load, (b) constant impedance load, and (c) ZIP load.

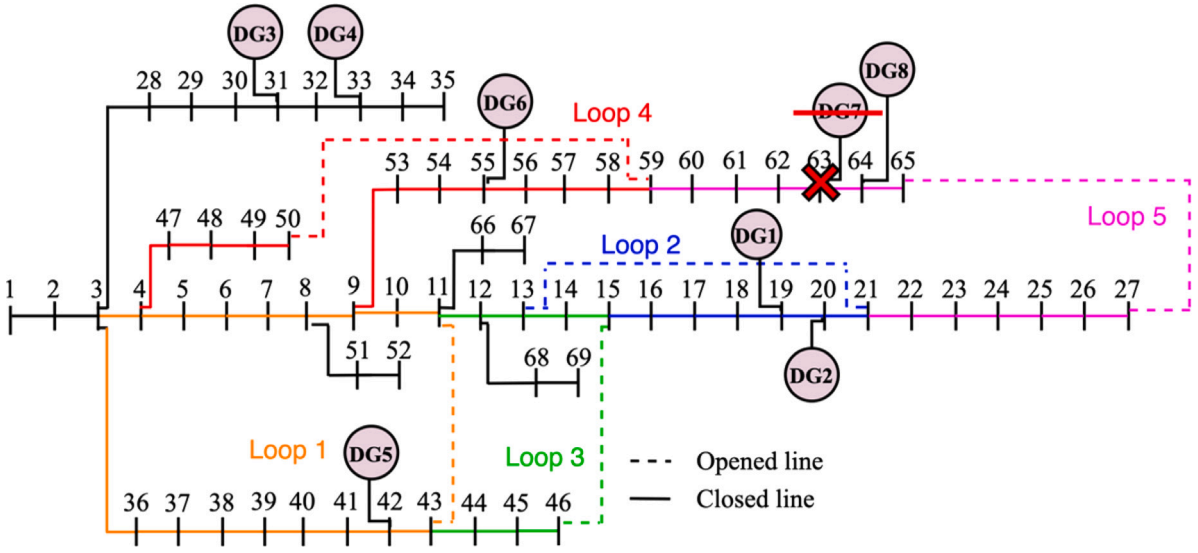

Fig. 4. Isolated IEEE – 69 bus system with additional DGs: Fault at bus 63.

Table 2
Unserved power for Case 1 (a): Grid-connected system without DGs.

Unserved power (MW)	Load type			
	Constant P	Constant I	Constant Z	ZIP load
Before reconfiguration	1.56	1.56	1.56	1.56
With reconfiguration	1.058	0.978	0.902	0.987
With reconfiguration & CVR	–	0	0	0.361

Table 3
Dispatchable DG size and location.

	Deterministic DGs							
Bus	19	20	31	33	42	55	63	64
DG size (kVA)	400	300	700	200	400	800	1400	600
$pf(min)$	0.7	0.7	0.7	0.7	0.7	0.7	0.7	0.7
n_q	3.5	4.67	2.04	7.14	3.57	1.785	1.003	2.33
m_p	0.4075	0.543	0.233	0.815	0.4075	0.2037	0.166	0.272

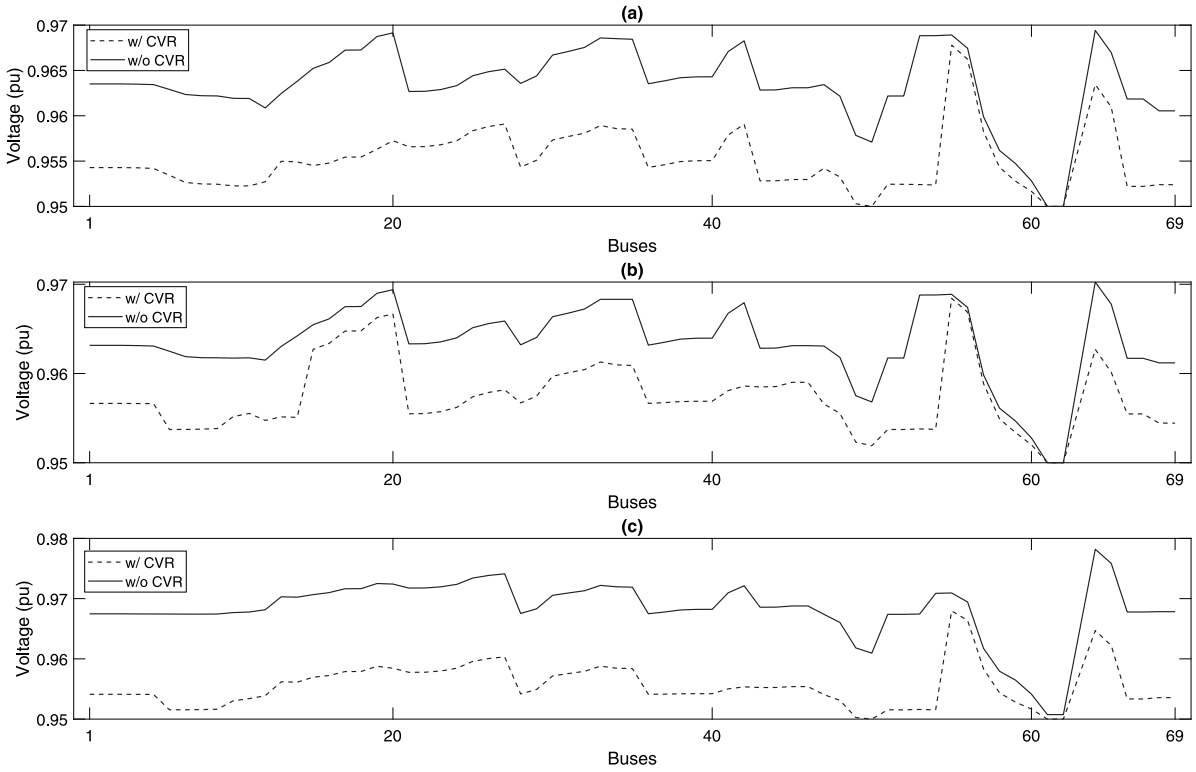

Fig. 5. Case 2 voltage profile for: (a) constant current loads, (b) constant impedance loads, and (c) ZIP loads.

Table 4
Unserved power for Case 1 (b): Grid-connected system with DGs.

Unserved power (MW)	Load type			
	Constant P	Constant I	Constant Z	ZIP load
Before reconfiguration	0.286	0.286	0.286	0.286
With reconfiguration	0	0	0	0
With reconfiguration & CVR	–	–	–	–

60 is examined for this case, as shown in Figs. 1 & 2. The fault has rendered the lines connected to bus 60 as open lines and cannot be used to reroute power during reconfiguration. This case study is split into two parts: Case 1 (a) without DGs and Case 1 (b) with DGs. In Case 1 (a), the sole power source in the system is the main grid which feeds the whole system. In Case 1 (b), a number of dispatchable DGs are assumed to be connected to the system and operate in constant PQ mode (grid–following), as depicted in Fig. 2.

3.1.1. Case 1 (a): Grid-connected system without DGs

A fault on bus 60 has been examined in this case on a system that is dominated with different load types as shown in Table 2. The load types that dominate the system might affect on the results of reconfiguration and the effectiveness of CVR in restoring the unserved loads. Furthermore, Fig. 3 displays CVR's effect on the voltage profile of the various load types in this case, excluding the constant power loads at which CVR was not deployed. Additionally, The power lost after the fault isolation and before reconfiguration is found using the constant power load model and is assumed the same for all load types examined due to the absence of voltage in the disconnected loads. In cases that reconfiguration is able to recover the full load, CVR is not deployed. Table 2 reflects that due to the fault location being close to a large load in the system, 1.244 MW at bus 61, the reconfiguration process alone was unable to recover the entire lost loads for any of the load types examined. Reconfiguration's ability to reroute power is limited by the voltage constraints and thermal limits present in the system. Therefore, reconfiguration-CVR fusion was deployed for load types that are voltage dependent in an attempt to serve more loads. The results in the table show that the fusion was able to recover the entire load for systems dominated with constant current by changing the tap on the OLTC to (−8 taps) and impedance loads by changing the tap on the OLTC to (−7 taps) accordingly. However, systems dominated with ZIP loads have seen significant reduction in unserved power using the reconfiguration-CVR fusion by changing the tap on the OLTC to (−8). Regardless of the new voltage operating point at bus 1, a portion of the load was left unserved in case of ZIP load. It is noteworthy to point out that ZIP modeled load contains a portion of load that is voltage independent hence, CVR could not recover the load fully.

3.1.2. Case 1 (b): Grid-connected system with DGs

This case study examines the same fault in Case 1 (a) with an addition of 8 dispatchable DGs connected to the network as shown in Fig. 2. The 8 DGs have been extracted from [20] which proposes optimum DGs sizes and locations catered to an isolated IEEE 69 – bus system. The DGs added are defined in Table 3. The presence of DGs in the system distributed the power injections within the system, noting that the DGs in this case are controlled in PQ mode and the grid solely controls the frequency and voltage setpoints of the system. The results of this case are shown in Table 4. The results reflect that reconfiguration alone is capable of retrieving the disconnected load in all load types in cases with high penetration DGs. As such, CVR has not been deployed in any of the load types and has no role in this case as opposed to Case 1 (a) where CVR was needed. Here, it is noteworthy that CVR could still be applied after the load restoration process to achieve other objectives, e.g., power loss minimization, however this is outside the scope of this work, which focuses on investigating the effectiveness of CVR to help recovering more loads during the restoration process.

3.2. Case 2: Isolated IEEE - 69 bus system

The second case examines a fault on bus 63 in an isolated system supplied by dispatchable DGs as described in Table 3, and shown

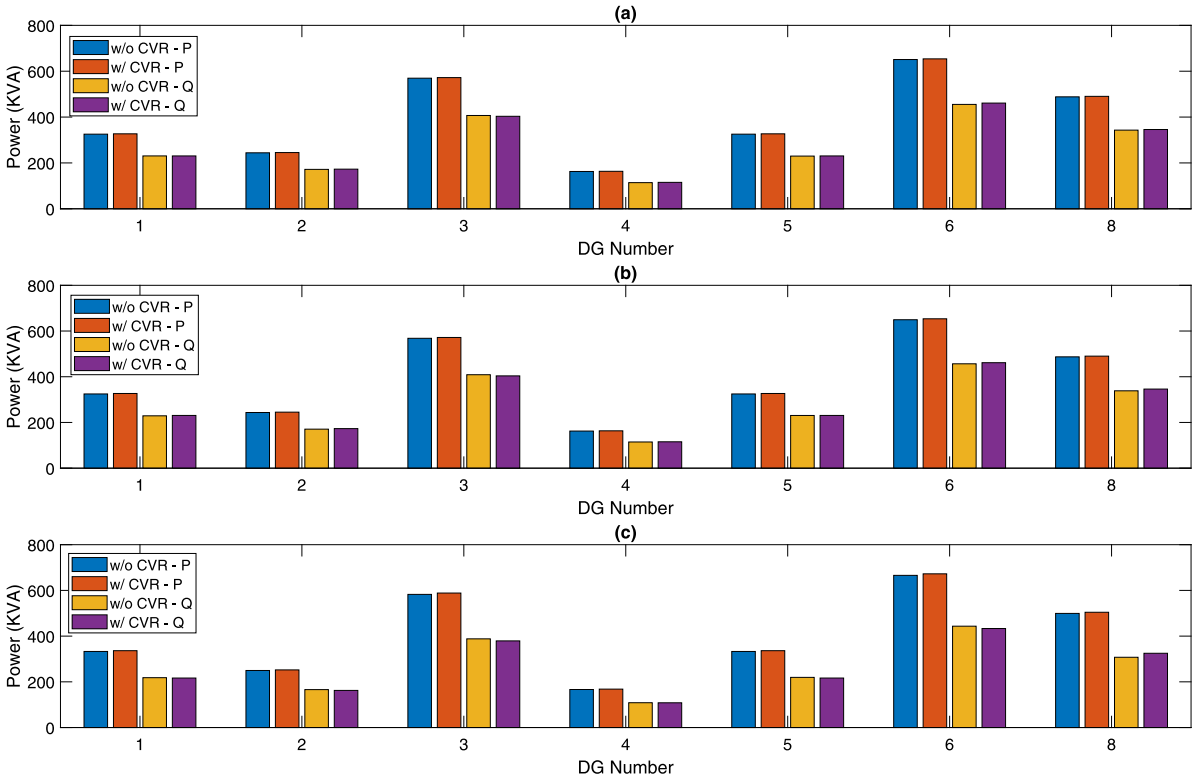

Fig. 6. Active and reactive power output of DGs in Case 2 for: (a) constant current load, (b) constant impedance load, and (c) ZIP load.

Table 5
Results for Case 2, isolated system.

Unserved power (MW)	Load type			
	Constant P	Constant I	Constant Z	ZIP load
Before reconfiguration	2.182	2.182	2.182	2.182
With reconfiguration	1.056	0.899	0.752	0.918
With reconfiguration & CVR	–	0.866	0.708	0.865

Table 6
Nominal voltage droop parameter for each DG in Case 2.

$\upsilon_{DG,i}^{s,nom}$	Load type		
	Constant I	Constant Z	ZIP load
DG1	1.0437	1.0465	1.0322
DG2	1.0443	01.047	1.0333
DG3	1.0386	1.0416	1.0337
DG4	1.0398	1.0428	1.035
DG5	1.0365	1.0427	1.0347
DG6	1.0485	1.0486	1.0438
DG8	1.0396	1.044	1.0394

in Fig. 4. Droop control is used to coordinate equal power sharing between the available DGs following Eqs. (17)–(21). The fault on bus 63 results in the loss of DG7 in this case, as shown in Fig. 4, causing the system to be deficient in generation. The results of this case are presented in Table 5 & Fig. 5. As shown in the table, the unserved load is significantly higher in this case than in the previous case/s due to a loss of key generation that the system depended on as opposed to the previous grid-connected case. Reconfiguration in this case has less effect on restoring loads than previous cases due to the added limitation, e.g., generation limitation to the system. The reconfiguration-CVR fusion has improved the performance of the restoration process by decreasing the unserved power demand compared to reconfiguration alone in most load types that are voltage dependent. The fusion effect on the voltage profile of different load types is evident in Fig. 5. The figure, Fig. 6, shows that DGs in the system share the active and reactive power of the system load based on their ratings and droop parameter settings. [22] describes this behavior as a plug-and-play feature, allowing decentralized control, droop control, to determine the frequency and voltage setpoints of the system. As shown in Fig. 6 the output active and reactive powers of the DGs during reconfiguration and reconfiguration with CVR are very similar. It is worth noting that DG7 is not included in Fig. 6 as it is no longer connected to the system. During reconfiguration, the nominal voltage setpoint of the droop parameters, $\upsilon_{DG,i}^{s,nom}$, is set at the upper bound = 1.05 pu. Meanwhile, to apply the CVR fusion, the parameter is left to be optimized by the optimizer and its optimal values are stated in Table 6. These values allowed CVR to be effective in the voltage dependent load types and minimize the unserved power with up to 5.77% in this case. The table also shows that the ZIP load demands the lowest voltage setpoints from the DGs while constant current and constant impedance load types are interchangeable in their associated nominal voltage setpoints.

3.3. Case 3: Isolated IEEE - 69 bus system with a mix of deterministic and variable DGs

This case examines a probabilistic approach by connecting variable wind turbines alongside the dispatchable DGs and modeling probabilistic load to the system. Before carrying out the case study, the details of the probabilistic generation and load must be defined. Introducing probabilistic wind turbine approach allows the examination of the effect of different weather conditions on the system [29]. The following subsections define the specifics of the probabilistic wind states, load states and indices used to analyze this case study.

3.3.1. Probabilistic wind turbine

The probabilistic nature of the wind is modeled using a Rayleigh PDF, which is commonly used to model the wind speed characteristics [30]. The PDF has been established using historical data spanning several years. To find the range between the probabilities, the PDF

Table 7
Annual wind and power states.

State	Wind speed	% Peak wind	Probability	Hour/year
1	14–25	100	0.078425	687
2	13–14	95	0.025	219
3	12–13	85	0.032648	286
4	11–12	75	0.045091	395
5	10–11	65	0.050114	439
6	9–10	55	0.077284	677
7	8–9	45	0.09121	799
8	7–8	35	0.112215	983
9	6–7	20	0.103653	908
10	5–6	15	0.112329	984
11	4–5	5	0.066096	579
12	0–4 & ≥25	0	0.205936	1804

Table 8
Wind turbine characteristics.

Scale parameters	c	$1.128 \times V^s_{aw}$
Shape parameters	k	2
Cut in speed	V^s_{ci}	4 m/s
Rated speed	V^s_r	14 m/s
Cut out speed	V^s_{co}	25 m/s

is integrated to find the cumulative density function (CDF). The wind speed is divided into 12 states. The first state considers the wind speeds between 14 m/s to 25 m/s to represent the wind turbine at rated power, then the following ten states consider the wind speed with a decreasing step of 1 m/s, and the last step considers wind speeds between 0 m/s–4 m/s and above 25 m/s. The wind states, probabilities, and power output associated are demonstrated using Table 7 [30]. The mean wind speed of each state, V^s_{aw}, is used to find the power output of that state. This means that, for example, state 2 includes all wind speeds between 13 m/s and 14 m/s, and the power output of that state is calculated for the mean wind speed of 13.5 m/s, and then assumed to be fixed for the whole range/state.

3.3.2. Probabilistic model details

Similar probabilistic analysis also needs to be considered for the load profile. The load is not always fixed or at peak load; In this case, the peak load is assumed to change following the hourly load shape of the IEEE - RTS. As a result, 10 states have been used to model the load profile, each state has the load operating at a different percentage of the peak load, as shown in Table 9 [31].

3.3.3. Combined generation - Load model

The combined generation-load model is found by convolving the probability of the wind states (12 states) by the probability of the load states (10 states), yielding 120 states in total. The combined probability is calculated using Eq. (22).

$$P(C^s) = P^s_w(t) \times P^s_l(L) \tag{22}$$

where for each state s, $P(C^s)$ is the combined probability of the state, $P^s_w(w)$ is wind probability of wind turbine w and $P^s_l(L)$ is the probability of the load L. The wind output power and load consumption for each state s is derived from the C matrix. The C matrix is a matrix composed of rows representing states and columns representing the w wind turbines in addition to, the total load. The different wind percentage of peak power is stored in the wth column of the C matrix. The different load states are stored in the w+1 column of the C matrix [30]. Each state has an associated percentage of the peak power output for wind turbines in the network and the percentage of the peak load for that state.

Table 9
Annual load and power states.

State	% Peak load	Probability	Hour/year
1	100	0.01	87.6
2	85.3	0.056	490.56
3	77.4	0.1057	925.93
4	71.3	0.1654	1448.9
5	65	0.1654	1448.9
6	58.5	0.163	1427.88
7	51	0.163	1427.88
8	45.1	0.0912	798.9
9	40.6	0.0473	414.35
10	35.1	0.033	289.1

Table 10
DG mix size and location.

	Deterministic						Wind	
Bus	19	20	33	42	55	63	31	64
DG size (kVA)	400	300	200	400	800	1400	700	600
$pf(min)$	0.7	0.7	0.7	0.7	0.7	0.7	1	1

Table 11
Case 3 results - unserved energy of different load types.

	Load type			
Energy lost	Constant P	Constant I	Constant Z	ZIP load
ENS (MWh/Year)	9060.1	9060.1	9060.1	9060.1
COST (k$/Year)	959.46	959.46	959.46	959.46
With reconfiguration	Constant P	Constant I	Constant Z	ZIP load
ENS (MWh/Year)	4850.75	4409.17	3392.87	3923.5
COST (k$/Year)	513.69	466.93	359.31	415.5
With reconfiguration & CVR	Constant P	Constant I	Constant Z	ZIP load
ENS (MWh/Year)	–	4050.14	3278.04	3708.57
COST (k$/Year)	–	428.91	347.14	392.74
Savings	–	8.1%	3.38%	5.478%

3.3.4. Indices used - Probabilistic analysis

The Cost of Energy Not Served (COST) and Energy Not Served (ENS) are indices used in this case to reflect an annual analysis. Eq. (23) formulates the ENS as the summation of unserved energy over all the states. The COST index in Eq. (24) translates the energy into dollar cost using the retail price of electricity, 10.59 cents/kWh. The price is based on the average retail price of electricity in the United States of America (USA) as presented by the U.S. Energy Information Administration (EIA) for the year 2020 [31].

$$ENS = \sum_{s=1}^{m} \sum_{i=1}^{n} P^s_{US,i} \times t^s \tag{23}$$

$$COST = ENS \times \mu \tag{24}$$

where t^s is the time that the state occurred within a year and μ is the retail price of electricity in $/kWh.

3.3.5. Case 3: Isolated IEEE - 69 system with a mix of dispatchable & probabilistic DGs - Results

The non-dispatchable DGs used in this case are wind turbines whose characteristics are defined in Table 8 [30] with a mean wind speed of 6.07 m/s in the site under study. This case is similar to Case 2, isolated system with DGs. The main difference is that two of the dispatchable DGs have been replaced by non-dispatchable wind turbines, the new DG mix is defined in Table 10 and shown in Fig. 7. All the 120 states, defined in the subsections above are analyzed with their associated wind and load peak percentage. This case will cover an annual period of 8760 h. The following indices: ENS (MWh/year) and COST (k$/year), defined in Eqs. (23) and (24), have been used to analyze and compare the results between the operation of reconfiguration alone and reconfiguration-CVR fusion. The total capacity of the deterministic DGs is 3500 kVA, and the WTs capacity is 1200 kVA. The total size of

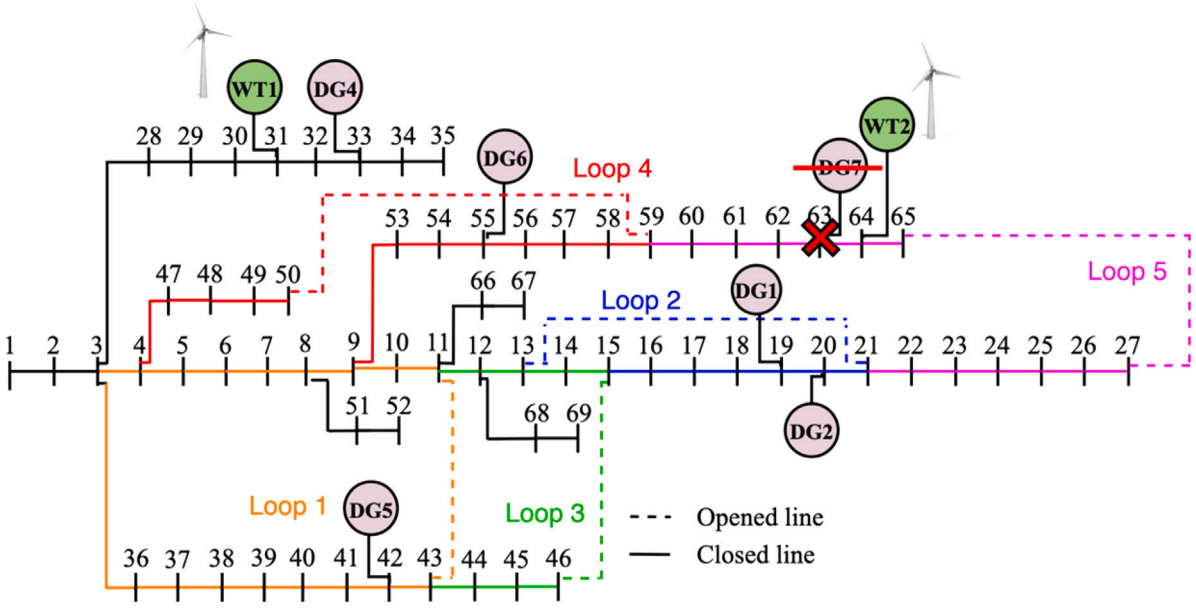

Fig. 7. Isolated IEEE – 69 bus system with dispatchable DGs and probabilistic WTs: Fault at bus 63.

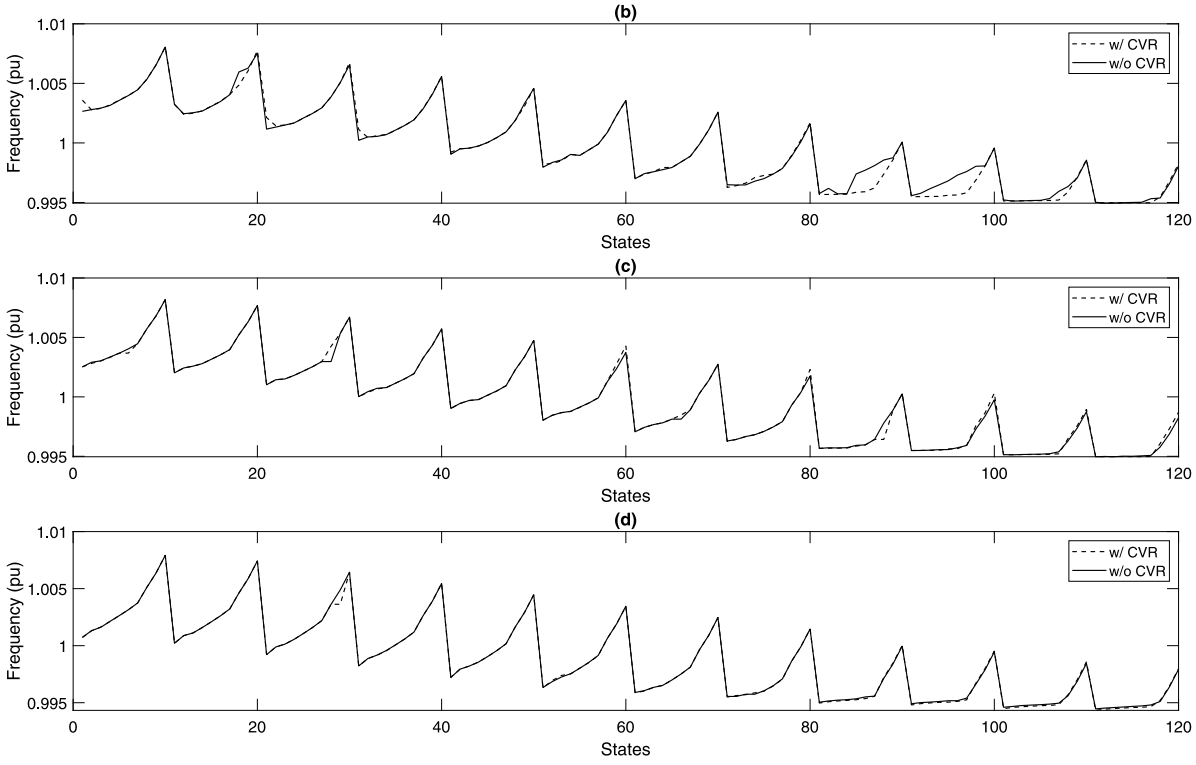

Fig. 8. Frequency of all 120 states for: (a) constant current load, (b) constant impedance load, and (c) ZIP load.

the DGs in the system is 4800 kVA; therefore, it covers the total load of 4650 kVA when the wind and load are at maximum capacity. The wind turbines operate at unity power factor and directly inject their output into the system. Due to the unity power factor, the total WT injection is 1200 kW at rated power. This ensures that the maximum wind injection is less than the minimum load state, 35.1% of active peak load being 1337 kW. This is done to avoid reverse power flow in the state that corresponds to 100% peak wind output and 35.1% peak load consumption. The same fault as case 2, is examined in this case, fault at bus 63. The fault is examined for all the 120 states. The frequency of the system in all the 120 states during reconfiguration alone and reconfiguration-CVR fusion can be seen in Fig. 8. This case considers energy lost instead of power lost as in previous cases due to the probabilistic analysis done in this case. The result of the fault on different load types is displayed in Table 11. The energy lost is large due to a loss in generation in addition to the probabilistic changes in wind output i.e., it is not injecting rated power in every state. In every load type, reconfiguration was able to recover a significant portion of the unserved energy, but the reconfiguration-CVR fusion was able to optimize the reconfiguration operation significantly, up to 8% in some

cases. Translating to an overall $590,000 reduction in cost annually in some load types, making the fusion of reconfiguration and CVR very attractive.

4. Conclusion

This paper proposes a new approach to enhance the power distribution system resilience by optimizing the self-healing scheme through the integration of CVR with system reconfiguration. The proposed optimization approach is formulated mathematically with consideration of different load types (constant power, current, impedance, and ZIP) and different operation modes (grid-connected and isolated). To validate the superiority and effectiveness of the proposed approach, several case studies have been carried out on the 69–bus distribution system: grid-connected without and with DG integration, isolated system with dispatchable DGs, and isolated system with a mix of dispatchable and non-dispatchable DGs. The cases have been carried out for reconfiguration alone and for the proposed reconfiguration-CVR fusion. The results showed that, depending on the load type and penetration levels of DGs, reconfiguration alone might be capable of restoring the entire load in grid-connected systems without the need of being integrated with CVR. Also, it has become clear from the case studies that the process of reconfiguration alone might fail short to restore the entire unserved load when a significant portion of generation and/or load is lost due to the imposed system's limitations; especially in cases of isolated systems. In all cases, reconfiguration alone recovered a significant portion of the lost loads; however, when compared to the reconfiguration-CVR fusion, the fusion was successful in freeing 3%–6% of energy and, thus, help restoring more loads. Further, in the final case study, a probabilistic analysis has been conducted to account for the variability of non-dispatchable power generation and load consumption in evaluating the effectiveness of the proposed approach. The results showed that a potential accumulated saving for the expected energy not served and the cost of outage in the range of 3%–8% could be achieved with the application of the proposed reconfiguration–CVR approach.

Declaration of competing interest

The authors declare that they have no known competing financial interests or personal relationships that could have appeared to influence the work reported in this paper.

Data availability

Data will be made available on request

Acknowledgments

This research is supported by ASPIRE, the technology program management pillar of Abu Dhabi's Advanced Technology Research Council (ATRC), ASPIRE "ViP (Visiting International Professorship)" Award. Under project with number VIP21-002.

References

[1] Beard LM, Cardell JB, Dobson I, Galvan F, Hawkins D, Jewell W, Kezunovic M, Overbye TJ, Sen PK, Tylavsky DJ. Key technical challenges for the electric power industry and climate change. IEEE Trans Energy Convers 2010;25(2):465–73. http://dx.doi.org/10.1109/TEC.2009.2032578.

[2] Borghei M, Ghassemi M. Optimal planning of microgrids for resilient distribution networks. Int J Electr Power Energy Syst 2021;128:106682. http://dx.doi.org/10.1016/j.ijepes.2020.106682.

[3] chen Zhou Z, Wu Z, Jin T. Deep reinforcement learning framework for resilience enhancement of distribution systems under extreme weather events. Int J Electr Power Energy Syst 2021;128:106676. http://dx.doi.org/10.1016/j.ijepes.2020.106676.

[4] Lin Y, Bie Z. Tri-level optimal hardening plan for a resilient distribution system considering reconfiguration and DG islanding. Appl Energy 2018;210:1266–79. http://dx.doi.org/10.1016/j.apenergy.2017.06.059.

[5] Zidan A, Khairalla M, Abdrabou AM, Khalifa T, Shaban K, Abdrabou A, El Shatshat R, Gaouda AM. Fault detection, isolation, and service restoration in distribution systems: State-of-the-art and future trends. IEEE Trans Smart Grid 2017;8(5):2170–85. http://dx.doi.org/10.1109/TSG.2016.2517620.

[6] Kleinberg MR, Miu K, Chiang H-D. Improving service restoration of power distribution systems through load curtailment of in-service customers. IEEE Trans Power Syst 2011;26(3):1110–7. http://dx.doi.org/10.1109/TPWRS.2010.2080327.

[7] Cavalcante PL, López JC, Franco JF, Rider MJ, Garcia AV, Malveira MRR, Martins LL, Direito LCM. Centralized self-healing scheme for electrical distribution systems. IEEE Trans Smart Grid 2016;7(1):145–55. http://dx.doi.org/10.1109/TSG.2015.2454436.

[8] Khomami MS, Jalilpoor K, Kenari MT, Sepasian MS. Bi-level network reconfiguration model to improve the resilience of distribution systems against extreme weather events. IET Gener Transm Distrib 2019;13(15):3302–10. http://dx.doi.org/10.1049/iet-gtd.2018.6971.

[9] Ding T, Lin Y, Bie Z, Chen C. A resilient microgrid formation strategy for load restoration considering master-slave distributed generators and topology reconfiguration. Appl Energy 2017;199:205–16. http://dx.doi.org/10.1016/j.apenergy.2017.05.012.

[10] Kumar Y, Das B, Sharma J. Multiobjective, multiconstraint service restoration of electric power distribution system with priority customers. IEEE Trans Power Deliv 2008;23(1):261–70. http://dx.doi.org/10.1109/TPWRD.2007.905412.

[11] Romero R, Franco JF, Leão FB, Rider MJ, de Souza ES. A new mathematical model for the restoration problem in balanced radial distribution systems. IEEE Trans Power Syst 2016;31(2):1259–68. http://dx.doi.org/10.1109/TPWRS.2015.2418160.

[12] Elmitwally A, Elsaid M, Elgamal M, Chen Z. A fuzzy-multiagent self-healing scheme for a distribution system with distributed generations. IEEE Trans Power Syst 2015;30(5):2612–22. http://dx.doi.org/10.1109/TPWRS.2014.2366072.

[13] Wang Z, Wang J. Self-healing resilient distribution systems based on sectionalization into microgrids. IEEE Trans Power Syst 2015;30(6):3139–49. http://dx.doi.org/10.1109/TPWRS.2015.2389753.

[14] Mahdi M, Genc VMI. A real-time self-healing methodology using model- and measurement-based islanding algorithms. IEEE Trans Smart Grid 2019;10(2):1195–204. http://dx.doi.org/10.1109/TSG.2017.2760698.

[15] Du Y, Tu H, Lu X, Wang J, Lukic S. Black-start and service restoration in resilient distribution systems with dynamic microgrids. IEEE J Emerg Sel Top Power Electron 2022;10(4):3975–86. http://dx.doi.org/10.1109/JESTPE.2021.3071765.

[16] Ding T, Wang Z, Qu M, Wang Z, Shahidehpour M. A sequential black-start restoration model for resilient active distribution networks. IEEE Trans Power Syst 2022;37(4):3133–6. http://dx.doi.org/10.1109/TPWRS.2022.3164589.

[17] Cadini F, Agliardi GL, Zio E. Estimation of rare event probabilities in power transmission networks subject to cascading failures. Reliab Eng Syst Saf 2017;158:9–20. http://dx.doi.org/10.1016/j.ress.2016.09.009, Special Sections: Reliability and Safety Certification of Software-Intensive Systems.

[18] Phadke A, Thorp J. Expose hidden failures to prevent cascading outages [in power systems]. IEEE Comput Appl Power 1996;9(3):20–3. http://dx.doi.org/10.1109/67.526849.

[19] Wang Z, Wang J. Review on implementation and assessment of conservation voltage reduction. IEEE Trans Power Syst 2014;29(3):1306–15. http://dx.doi.org/10.1109/TPWRS.2013.2288518.

[20] Gupta Y, Nellikkath R, Chatterjee K, Doolla S. Volt–Var optimization and reconfiguration: Reducing power demand and losses in a droop-based microgrid. IEEE Trans Ind Appl 2021;57(3):2769–81. http://dx.doi.org/10.1109/TIA.2021.3057008.

[21] IEEE guide for identifying and improving voltage quality in power systems. IEEE Std 1250-2018 (Revision of IEEE Std 1250-2011), 2018, p. 1–63. http://dx.doi.org/10.1109/IEEESTD.2018.8532376.

[22] Hamad B, Al-Durra A, EL-Fouly THM, Zeineldin HH. Economically optimal and stability preserving hybrid droop control for autonomous microgrids. IEEE Trans Power Syst 2023;38(1):934–47. http://dx.doi.org/10.1109/TPWRS.2022.3169801.

[23] Elsayed WT, Farag H, Zeineldin HH, El-Saadany EF. Dynamic transitional droops for seamless line-switching in islanded microgrids. IEEE Trans Power Syst 2021;36(6):5590–601. http://dx.doi.org/10.1109/TPWRS.2021.3069852.

[24] Brooke A, Kendrick D, Meeraus A, Raman R, Rosenthal R. GAMS - A user's guide. 1st ed.. GAMS Development Corporation; 1998.

[25] Savier JS, Das D. Impact of network reconfiguration on loss allocation of radial distribution systems. IEEE Trans Power Deliv 2007;22(4):2473–80. http://dx.doi.org/10.1109/TPWRD.2007.905370.

[26] Gilvanejad M, Askarian Abyaneh H, Mazlumi K. Estimation of cold-load pickup occurrence rate in distribution systems. IEEE Trans Power Deliv 2013;28(2):1138–47. http://dx.doi.org/10.1109/TPWRD.2012.2231967.

[27] Baran M, Wu F. Optimal capacitor placement on radial distribution systems. IEEE Trans Power Deliv 1989;4(1):725–34. http://dx.doi.org/10.1109/61.19265.

[28] Bokhari A, Alkan A, Dogan R, Diaz-Aguiló M, de León F, Czarkowski D, Zabar Z, Birenbaum L, Noel A, Uosef RE. Experimental determination of the ZIP coefficients for modern residential, commercial, and industrial loads. IEEE Trans Power Deliv 2014;29(3):1372–81. http://dx.doi.org/10.1109/TPWRD.2013.2285096.

[29] Distributed energy resources on distribution networks: A systematic review of modelling, simulation, metrics, and impacts. Int J Electr Power Energy Syst 2022;138:107900. http://dx.doi.org/10.1016/j.ijepes.2021.107900.

[30] Atwa Y, El-Saadany E. Probabilistic approach for optimal allocation of wind-based distributed generation in distribution systems. Renew Power Gener IET 2011;5:79–88. http://dx.doi.org/10.1049/iet-rpg.2009.0011.

[31] Pinheiro J, Dornellas C, Schilling M, Melo A, Mello J. Probing the new IEEE Reliability Test System (RTS-96): HL-II assessment. IEEE Trans Power Syst 1998;13(1):171–6. http://dx.doi.org/10.1109/59.651632.